Gravitational lensing of charged Ayon-Beato-Garcia black holes and non-linear effects of Maxwell fields

H. Ghaffarnejad¹, M. A. Mojahedi² and H. Niad ³ Faculty of Physics, Semnan University, Zip Code 35131-19111, Iran

Abstract

Non-singular Ayon-Beato-Garcia (ABG) spherically symmetric sta tic black hole (BH) with charge to mass ratio $q = \frac{g}{2m}$ is metric solution of Born-Infeld nonlinear Maxwell-Einstein theory. Central region of the BH behaves as (anti-) de Sitter for (|q| > 1) |q| < 1. In case of |q| = 1 the BH central region behaves as Minkowski flat metric. Nonlinear Electromagnetic (NEM) fields counterpart causes to deviate light geodesics and so light rays will forced to move on effective metric. In this paper we study weak and strong gravitational lensing of light rays by seeking affects of NEM fields counterpart on image locations and corresponding magnification. We set our calculations to experimentally observed Sgr A* BH. In short we obtained: For large distances the NEM counterpart is negligible reaching to linear Maxwell fields. The NEM makes enlarge the BH photon sphere radius as linearly by raising |q| > 1 but deceases by raising $|q| \le 1$. Sign of deflection angle of bending light rays is changed in presence of NEM effects with respect to ones obtained in absence of NEM fields. Absolute value of deflection angle raises by increasing $|q| \to 1$. Weak image locations decreases (increases) by raising 0 < |q| < 1 in presence (absence) of NEM fields. By raising the closest distance of the bending light rays weak image locations changes from left (right) to right (left) in absence (presence) of NEM fields. Einstein rings radius and corresponding magnification centroid become larger (smaller) in presence (absence) of NEM fields in case of weak lensing. Angular separation s between the innermost and outermost relativistic images increases (decreases) by increasing 0 < |q| < 1 in absence (presence) of NEM fields. Corresponding magnification r decreases (increases) by raising 0 < |q| < 1 in absence (presence) of NEM fields. s(r) raises (decreases) by increasing |q| >> 1.

¹E-mail address: hghafarnejad@semnan.ac.ir ²E-mail address: amirmojahed@semnan.ac.ir

³E-mail address: niad@semnan.ac.ir

1 Introduction

Since the advent of Einstein's general relativity theory, black holes and the singularity problem of curved space times become challenging subjects in modern physics because of presence of quantum physics. Singularity is the intrinsic character of the most exact solutions of Einstein's equations where Ricci and Kretschmann scalars reach to infinite value at singular point of the space time [1]. Penrose cosmic censorship conjecture states that the causal singularities must be covered by the event horizon and so causes to disconnect interior and exterior regions of the space time [2,3]. However nonsingular metric solutions are also obtained from the Einstein field equation (see for instance [4-23]). In the latter situations the Einstein field equation is coupled to suitable NEM fields for which the Ricci and the Kretschmann scalars become regular in whole space time. A good classification of spherically symmetric static regular black holes are collected in ref. [9]. Inspiring a physical central core idea, Bardeen suggested the first spherically symmetric static regular black hole in 1968 containing a horizon without singularity [10]. After his work, other regular black holes were designed based on this model which we call here for instance ABG [11-14], Hayward (HAY) [15] and Neves-Saa (NS) [16,17]. Non-singular property of all of these solutions are controlled via dimensionless charge parameter q. HAY type of regular black hole is obtained by modifying the mass parameter of the BAR black hole. NS type of regular black hole is a HAY type but its asymptotic behavior approaches to a vacuum de Sitter in presence of cosmological constant parameter. Regular black holes are studied also on brane words (see [17] and reference therein). The solutions of rotating regular black holes have been introduced in several articles [18-24]. A very important source of strong gravity is the Kerr-Newman-de Sitter (KNDS) and/or Kerr-Newman- anti-de Sitter (KNADS) black hole. Kraniotis studied gravitational lensing of KNDS and KNADS black hole in ref. [25], where closed form analytic solutions of the null geodesics and the gravitational lens equations have been obtained in terms of Appell-Lauricella generalized hypergeometric functions and the elliptic functions of Weierstrass. In these exact solutions all the fundamental parameters of the theory, namely black hole mass, electric charge, rotation angular momentum and the cosmological constant enter on an equal footing while the electric charge effect on relativistic observable was also investigated. Rotating nonsingular black holes can be treat as natural particle accelerators [24]. Ultra-high energy particle collisions are studied on the regular black holes [26] and backgrounds containing naked singularity [27]. Motion of test particles is studied in regular black hole spacetimes in ref. [28]. Circular geodesics are obtained for BAR and ABG regular black-holes in ref. [29]. The optical effects related to Keplerian discs orbiting Kehagias-Sfetsos (KS) naked singularities was investigated in ref. [30]. Authors of the latter work are also mentioned to be close similarity between circular geodesics in KS and properties of the circular geodesics of the RN naked singular space times. Schee et al studied also profiled spectral lines generated by keplerian discs orbiting in the Bardeen and ABG space times in ref. [31]. Correspondence between the black holes and the FRW geometries are studied for non-relativistic gravity models in ref. [32]. RN black hole gravitational lensing is studied in ref. [33]. Gravitational lensing from regular black holes is studied in weak deflection limits of light rays [34-36] and in strong deflection limits of light rays [37-41]. Strong deflection limits of light rays can be distinguish gravitational lensing between naked singularity and regular black holes background [41]. There is significant difference between optical phenomena characters of the singular space-times such as SCH, RSN, and non-singular space-times as HAY, BAR, ABG [38]. It is related to the fact that the regular space-times reach to a de Sitter and/or anti-de Sitter like approximately at center $r \to 0$ (see Eqs. (2.7) and (2.9)). Furthermore we should point that the nonsingular charged black holes obtained from NEM models in curved space times cause that the photons do not move along null geodesics. As an applicable approach we must be obtain corresponding effective metric for geodesics of moving photons [42-45] and so study their gravitational lensing. The black hole electric charge has also important effects on final state of the Hawking radiation and switching off effects of a quantum evaporating black hole (see for instance [46]). In this work we study gravitational lensing of light rays moving on the ABG nonsingular black hole in presence of NEM fields counterparts. The paper is organized as follows.

Briefly, we introduce in section 2 regular ABG black hole metric and its asymptotically behavior against different values of q. In section 3 we calculate effective metric of the ABG black hole for the moving photons by regarding the results of the original work [12]. We solve numerically the photon sphere equation of effective metric and obtain photon sphere radius against different charge values q. In section 4 we evaluate general formalism of deflection angle of bending light rays in weak and strong deflection limits. In weak deflection limits we apply the Ohanian lens equation [47] to determine non-relativistic image locations against source positions for observed $\operatorname{Sgr} A^*$

black hole [48-51]. Weak deflection angle of bending light rays and their magnifications are evaluated numerically point by point and they are plotted against source locations and also q. In the strong deflection limits we use Bozza's formalism [37,38] to obtain logarithmic form of the deflection angle. We obtain relative distance between innermost and outermost relativistic images and corresponding magnification and then plot their diagrams. Section 5 denotes to concluding remark.

2 ABG space time

The ABG spherically symmetric black hole metric defined by Schwarzschild coordinates is [12]

$$ds^{2} = -H(r)dt^{2} + \frac{dr^{2}}{H(r)} + r^{2}(d\theta^{2} + \sin^{2}\theta d\varphi^{2})$$
 (2.1)

with

$$H(r) = 1 - \frac{2mr^2}{(r^2 + g^2)^{3/2}} + \frac{g^2r^2}{(r^2 + g^2)^2}$$
 (2.2)

and associated electric field

$$F_{tr}(r) = E(r) = gr^4 \left(\frac{r^2 - 5g^2}{(r^2 + g^2)^4} + \frac{15}{2} \frac{m}{(r^2 + g^2)^{\frac{7}{2}}} \right).$$
 (2.3)

m and g are total mass and electric charge parameters of the BH respectively. The line element (2.1) is non-singular static solution of NEM-Einstein metric equation

$$G_{\mu\nu} = 8\pi T_{\mu\nu} = 8\pi \{\mathcal{L}_F F_{\mu\eta} F^{\eta}_{\nu} - \mathcal{L} g_{\mu\nu}\}, \quad \mathcal{L}_F = \frac{\partial \mathcal{L}}{\partial F}$$
 (2.4)

which satisfies the action functional $I = \int \sqrt{g} dx^4 \left(\frac{R}{16\pi} - \frac{\mathcal{L}(F)}{4\pi}\right)$ where R is Ricci scalar and \mathcal{L} is a functional of $F = \frac{1}{4}F_{\mu\nu}F^{\mu\nu}$. This metric solution has only the coordinate singularity called as horizon singularity because the Ricci and the Kretschmann scalars become regular at all points of the space time $0 \le r \le +\infty$. Defining mass and charge functions as

$$M(r) = m\left(1 + \frac{g^2}{r^2}\right)^{-\frac{3}{2}}, \quad e(r) = g\left(1 + \frac{g^2}{r^2}\right)^{-1}$$
 (2.5)

one can show that the ABG metric (2.1) reduces apparently to a variable mass-charge RN type of BH as

$$ds^{2} = -\left(1 - \frac{2M(r)}{r} + \frac{e^{2}(r)}{r^{2}}\right)dt^{2} + \frac{dr^{2}}{\left(1 - \frac{2M(r)}{r} + \frac{e^{2}(r)}{r^{2}}\right)} + r^{2}(d\theta^{2} + \sin^{2}\theta d\varphi^{2})$$
(2.6)

where $M(\infty) = m$ and $e^2(\infty) = g$ are ADM mass and electric charge viewed from observer located at infinity. Its central region 0 < r < |g| behaves as vacuum de Sitter asymptotically:

$$ds^{2} \approx -\left(1 - \frac{\Lambda}{3}r^{2}\right)dt^{2} + \frac{dr^{2}}{\left(1 - \frac{\Lambda}{3}r^{2}\right)} + r^{2}(d\theta^{2} + \sin^{2}\theta d\varphi^{2})$$
 (2.7)

for

$$|q| = \frac{g}{2m} < 1 \tag{2.8}$$

and anti de Sitter

$$ds^{2} \approx -\left(1 + \frac{\Lambda}{3}r^{2}\right)dt^{2} + \frac{dr^{2}}{\left(1 + \frac{\Lambda}{3}r^{2}\right)} + r^{2}(d\theta^{2} + \sin^{2}\theta d\varphi^{2})$$
 (2.9)

for

$$|q| = \frac{g}{2m} > 1 \tag{2.10}$$

respectively where we defined effective cosmological constant as

$$\Lambda(m,g) = \frac{3(1-q)}{4m^2q^3}. (2.11)$$

In particular case

$$|q| = \frac{g}{2m} = 1 \tag{2.12}$$

the effective cosmological parameter vanishes $\Lambda=0$ and so near the center $r\to 0$, the ABG black hole metric reduces to a flat Minkowski background asymptotically. Setting g=0 the equations (2.5) read m=M, e=0 for which the metric solution (2.1) leads to singular charge-less Schwarzschild BH. Nonlinear counterpart of the Maxwell stress tensor causes to deviate the photon geodesics where the photons do not move along the null geodesics. Usually one use an effective metric to study gravitational lensing of the light rays moving on such a charged black holes metric [41-44]. In the following section we seek effective metric of the ABG black hole for photon trajectories.

3 Effective metric for photon trajectories

Assuming $\mathcal{L}(F) = F$, the equation (2.4) leads to the well known linear Einstein-Maxwell gravity where the photon propagates by the null equation

$$g_{\mu\nu}k^{\mu}k^{\nu} = 0 \tag{3.1}$$

where k^{μ} is corresponding four-momentum of the photon, but in general form where $\mathcal{L}(F) \neq F$ the electric field given by (2.3), is self-interacting and so directly is reflected on the photon propagation. In the latter case the photons do not move along null geodesics (3.1) but instead, photons propagate along null geodesics of an effective geometry which depends on used nonlinear theories [43,44,52] as

$$g_{\mu\nu}^{eff}k^{\mu}k^{\nu} = 0 \tag{3.2}$$

where

$$g_{\mu\nu}^{eff} = 16 \left(\frac{\mathcal{L}_{FF} F_{\mu\eta} F_{\nu}^{\eta} - (\mathcal{L}_F + 2F \mathcal{L}_{FF}) g_{\mu\nu}}{F^2 \mathcal{L}_{FF}^2 - 16 (\mathcal{L}_F + F \mathcal{L}_{FF})^2} \right)$$
(3.3)

and

$$g_{eff}^{\mu\nu} = \mathcal{L}_{FF} F_{\eta}^{\mu} F^{\nu\eta} + \mathcal{L}_F g^{\mu\nu}. \tag{3.4}$$

In absence of nonlinear counterpart of EM fields we must be set

$$\mathcal{L}_{FF} = 0, \quad \mathcal{L}_F = 1, \quad \mathcal{L} = F$$
 (3.5)

for which the effective metric reaches $g_{\mu\nu}^{eff} \to g_{\mu\nu}$. We are now in position to obtain effective metric of spherically symmetric static space time (2.1). To do so we must be obtain all quantities defined by $\{\mathcal{L}, \mathcal{L}_F, \mathcal{L}_{FF}\}$ which satisfy the metric solution (2.1). We should first obtain corresponding Lagrangian density $\mathcal{L}(F)$. We use result of the original paper [12] where its authors are used following ansatz to solve (2.4) and obtain (2.1).

$$F\mathcal{L}_F^2 = -\frac{1}{2(2m)^2} \frac{q^2}{x^4} \tag{3.6}$$

where

$$F(x) = -\frac{1}{(2m)^2} \frac{q^2 x^8}{2} \left[\frac{x^2 - 5q^2}{(x^2 + q^2)^4} + \frac{15}{4} \frac{1}{(x^2 + q^2)^{\frac{7}{2}}} \right]^2$$
(3.7)

comes from (2.3) by inserting dimensionless electric charge q and radial coordinate x

$$q = \frac{g}{2m}, \quad x = \frac{r}{2m} \tag{3.8}$$

into $F = \frac{1}{4}F_{\mu\nu}F^{\mu\nu}$. One can obtain asymptotically behavior of the equation (3.7) for large distances x >> 1 as $F_{\infty}(x) \approx -\frac{1}{2(2m)^2} \frac{q^2}{x^4}$. Comparing the latter result and (3.6) we infer $\mathcal{L}_F \approx 1$ which by integrating leads to linear Maxwell Lagrangian $\mathcal{L} \to F$. The latter result tells us NEM action functionals $\mathcal{L}(F)$ are negligible for regions of far from the black hole event horizon $x >> x_{EH}$. Applying (3.6) and (3.7) we obtain parametric form of the Lagrangian density $\mathcal{L}(x)$ as follows.

$$\mathcal{L}(x) = -\frac{q^2}{(2m)^2} \int_{\infty}^{x} \frac{1}{x^2} d\left\{ x^4 \left[\frac{x^2 - 5q^2}{(x^2 + q^2)^4} + \frac{15}{4} \frac{1}{(x^2 + q^2)^{\frac{7}{2}}} \right] \right\}$$
(3.9)

which has exact solution as

$$\mathcal{L}(x) = -\frac{q^2}{(2m)^2} \left[\frac{x^2(x^2 - 5q^2)}{(x^2 + q^2)^4} + \frac{15}{4} \frac{x^2}{(x^2 + q^2)^{\frac{7}{2}}} \right] +$$

$$\frac{q^2}{(2m)^2} \left[\frac{1}{2(x^2+q^2)^2} - \frac{2q^2}{(x^2+q^2)^3} + \frac{3}{2} \frac{1}{(x^2+q^2)^{\frac{5}{2}}} \right].$$
 (3.10)

One infers

$$\mathcal{L}_F(x) = \frac{\mathcal{L}'(x)}{F'(x)} \tag{3.11}$$

and

$$\mathcal{L}_{FF}(x) = \frac{1}{F'(x)} \left(\frac{\mathcal{L}'}{F'}\right)' = \frac{\mathcal{L}''F' - F''\mathcal{L}'}{F'^3}$$
(3.12)

where over-prime \prime denotes to differentiation with respect to x. If we need to obtain exact form of the functional $\mathcal{L}(F)$ we must be remove x between (3.7) and (3.10) but it will take more complex form. Hence we plot numerical diagram of $\mathcal{L}(F)$ by inserting numerical values of tables 1 and 2 in figure 1. The diagram shows that negligibility of NEM fields for |q| > 1 but not for |q| < 1. However we will need to exact form of the functions $\{\mathcal{L}(x), \mathcal{L}_F(x), \mathcal{L}_{FF}(x)\}$ to study location of effective metric horizons, gravitational lensing images and their magnifications. To do so we will use numerical method as follows. For metric solution (2.1) one can show that the effective metric (3.3) become

$$ds_{eff}^{2} = -A(r)dt^{2} + B(r)dr^{2} + r^{2}C(r)(d\theta^{2} + \sin^{2}\theta d\varphi^{2})$$
 (3.13)

where we defined

$$A(r) = \frac{16H(r)\mathcal{L}_F}{16(\mathcal{L}_F + F\mathcal{L}_{FF})^2 - F^2\mathcal{L}_{FF}^2}$$
(3.14)

$$B(r) = \frac{1}{H(r)} \frac{16\mathcal{L}_F}{16(\mathcal{L}_F + F\mathcal{L}_{FF})^2 - F^2\mathcal{L}_{FF}^2}$$
(3.15)

and

$$C(r) = \frac{8(2\mathcal{L}_F + 4F\mathcal{L}_{FF})}{16(\mathcal{L}_F + F\mathcal{L}_{FF})^2 - F^2\mathcal{L}_{FF}^2}.$$
 (3.16)

The radius of the event horizon r_H is given by the greatest positive root of the equation H(r) = 0(A(r) = 0) in absence (presence) of nonlinear counterpart of EM field. According to study of black hole gravitational lensing, photon sphere construction is one of important characters which must be considered here. It comes from energy condition [53] and is a particular hyper-surface (r = constant) which does not evolve with time. In other words any null geodesic initially tangent to the photon sphere hyper-surface will remain tangent to it. It is made from circulating photons turn turning around the black hole center. Radius of the photon sphere r_{ps} is the greatest positive solution of the equation [48]

$$\left(\frac{1}{r^2} \frac{A(r)}{C(r)}\right)'_{|_{r=r_{ps}^{eff}}} = 0.$$
 (3.17)

Setting (3.5) the equations (3.14), (3.15) and (3.16) read

$$A(r) = H(r), \quad B(r) = \frac{1}{H(r)}, \quad C(r) = 1$$
 (3.18)

describing original space time (2.1) in absence of the nonlinear EM fields effects for which (3.17) become

$$\left(\frac{H(r)}{r^2}\right)'_{|r=r_{ns}} = 0. \tag{3.19}$$

Diagrams of the equations (3.17) and (3.19) are plotted for larger solutions in figure 1. Linear branch of the right panel of diagram in figure 1 predicts large scale photon spheres for |q| > 1 which are formed only in presence of

NEM field. This linear branch of the effective photon sphere diagram can be approximated with the following equation.

$$x_{ps}^{eff}(|q| > 1) \approx 3.643|q| - 0.796$$
 (3.20)

which raises by increasing $|q| \to \infty$. We calculated numerical values of the above photon sphere radius for 1 < |q| < 36 and collected in the table 2. Corresponding diagram is given in figure 1. One can result from the figure 1 that we have small scale photon sphere for |q| < 1 from both of the effective metric (3.13) and the original one (2.1). Hence obtained gravitational lensing results from (2.1) can be compared with ones which obtained from (3.13) only for |q| < 1. Thus we collect numerical solutions of the both photon sphere equations (3.17) and (3.19) for |q| < 1 in table 1. We will need them to evaluate numerical values of deflection angle, image locations and corresponding magnifications. We will study gravitational lensing of the system separately for two regimes |q| > 1 and |q| < 1 as follows. We first apply to evaluate numerical values of the deflection angle of bending light rays.

4 Deflection angle

When light ray moves at neighborhood of the ABG black hole and deflects without turning around the black hole center then gravitational lensing takes 'weak deflection limits' approach. In the latter case closest approach distance of the bending light rays from the black hole center r_0 become larger than the photon sphere radius and two non-relativistic images are usually formed. They are called as primary and secondary images. In general, bending angle of light rays is obtained by solving null geodesics equation defined by (3.1) as follows [54].

$$\alpha_{eff}(r_0) = I_{eff}(r_0) - \pi \tag{4.1}$$

where

$$I_{eff}(x_0) = 2 \int_{x_0 > x_{ps}}^{\infty} \frac{\sqrt{A(x)B(x)/C^2(x)}}{\sqrt{\frac{A(x_0)}{x_0^2C(x_0)} - \frac{A(x)}{x^2C(x)}}} \frac{dx}{x^2}.$$
 (4.2)

Inserting

$$z = \frac{x_0}{x} \tag{4.3}$$

the integral equations (4.2) become

$$I_{eff}(x_0) = 2 \int_0^1 \frac{\Gamma(\frac{x_0}{z})}{\sqrt{\Omega(x_0) - \Omega(\frac{x_0}{z})z^2}} dz$$
 (4.4)

where we defined

$$\Gamma\left(\frac{x_0}{z}\right) = \Omega\sqrt{\frac{B}{A}} = \frac{\mathcal{L}_F}{\mathcal{L}_F + 2F\mathcal{L}_{FF}}, \quad \Omega\left(\frac{x_0}{z}\right) = \frac{A}{C} = H\Gamma$$
 (4.5)

According to method given in ref. [52], we now expand $\Gamma(\frac{x_0}{z})$ and $\Omega(x_0) - \Omega(\frac{x_0}{z})z^2$ in powers of (1-z) as follows.

$$\Gamma(\frac{x_0}{z}) = \Gamma_0 + \Gamma_1(1-z) + \Gamma_2(1-z)^2 + O(3)$$
(4.6)

and

$$\Omega(x_0) - \Omega(\frac{x_0}{z})z^2 = \Omega_1(1-z) + \Omega_2(1-z)^2 + O(3)$$
 (4.7)

where we defined

$$\Gamma_0 = \Gamma(x_0), \quad \Gamma_1 = x_0 \Gamma'(x_0), \quad \Gamma_2 = x_0 \Gamma'(x_0) + x_0^2 \Gamma''(x_0)/2$$
 (4.8)

and

$$\Omega_1 = 2\Omega(x_0) - x_0\Omega'(x_0), \quad \Omega_2 = x_0\Omega'(x_0) - \Omega(x_0) - x_0^2\Omega''(x_0)/2 \quad (4.9)$$

in which over-prime 'denotes to differentiation with respect to its argument x. Inserting (4.6) and (4.7) and neglecting their higher order terms, the integral equation (4.4) become

$$I_{eff}(x_0) \approx 2 \int_0^1 dz \left[\frac{\Gamma_0 + \Gamma_1(1-z) + \Gamma_2(1-z)^2}{\sqrt{\Omega_1(1-z) + \Omega_2(1-z)^2}} \right]$$
(4.10)

which has solution as follows.

$$I_{eff}(x_0) = \frac{1}{\sqrt{\Omega_2(x_0)}} \sqrt{1 + \frac{\Omega_1(x_0)}{\Omega_2(x_0)}} \left[2\Gamma_1(x_0) + \Gamma_2(x_0) - \frac{3}{2}\Gamma_2(x_0) \frac{\Omega_1(x_0)}{\Omega_2(x_0)} \right]$$
$$-\frac{1}{\sqrt{\Omega_2(x_0)}} \left[2\Gamma_0(x_0) - \Gamma_1(x_0) \frac{\Omega_1(x_0)}{\Omega_2(x_0)} + \frac{3}{4}\Gamma_2(x_0) \left(\frac{\Omega_1(x_0)}{\Omega_2(x_0)} \right)^2 \right]$$

$$\times \ln \left[1 + 2 \ frac \left(1 - \sqrt{1 + \frac{\Omega_1(x_0)}{\Omega_2(x_0)}} \right) \frac{\Omega_1(x_0)}{\Omega_2(x_0)} \right]$$
 (4.11)

Weak (strong) deflection limits of bending light rays are regimes where $I_{eff}(x_0) \rightarrow \infty (\rightarrow \infty)$. This restrict us to choose particular regimes of the ratio $\frac{\Omega_1}{\Omega_2}$ given by (4.11). Inserting (4.5) and (4.9) into the photon sphere equation (3.17) and setting $x_0 = x_{ps}^{eff}$ one can result $x_{ps}\Omega'(x_{ps}) - 2\Omega(x_{ps}) = \Omega_1(x_{ps}) = 0$. The latter condition is valid for moving light rays near the photon sphere for which $I_{eff} \rightarrow \infty$. In other words one infers $\Omega_1(x_0 \neq x_{ps}^{eff}) \neq 0$ for weak deflection limits and so we can use asymptotic expansion form of the integral solution (4.11) for $x_0 > x_{ps}$ and $\forall q$ as follows.

4.1 Weak lensing deflection angles

One can obtain asymptotic expansion series form of the functions $\Omega_{1,2}(x_0)$ and $\Gamma_{0,1,2}(x_0)$ which up to terms in order of $O(x_0^{-3})$ become respectively

$$\Omega_1(x_0) \approx 2 - \frac{\frac{3}{8}}{x_0} - \frac{(32q^2 + \frac{345}{8})}{x_0^2} + \frac{(\frac{4305q^2}{16} + \frac{25875}{128})}{x_0^3}$$
(4.12)

$$\Omega_2(x_0) \approx -1 + \frac{\frac{3}{8}}{x_0} + \frac{\left(\frac{1035}{16} + 48q^2\right)}{x_0^2} - \frac{\left(\frac{4305q^2}{8} + \frac{25875}{64}\right)}{x_0^3}$$
(4.13)

$$\Gamma_0(x_0) \approx 1 + \frac{\frac{15}{8}}{x_0} - \frac{(9q^2 + \frac{225}{32})}{x_0^2} + \frac{(\frac{495q^2}{16} + \frac{3375}{128})}{x_0^3}$$
(4.14)

$$\Gamma_1(x_0) \approx -\frac{\frac{15}{8}}{x_0} + \frac{(18q^2 + \frac{225}{16})}{x_0^2} - \frac{(\frac{1485q^2}{16} + \frac{10125}{128})}{x_0^3}$$
(4.15)

and

$$\Gamma_2(x_0) \approx -\frac{(9q^2 + \frac{225}{32})}{x_0^2} + \frac{(\frac{1485q^2}{16} + \frac{10125}{128})}{x_0^3}.$$
(4.16)

Inserting (4.12), (4.13), (4.14), (4.15) and (4.16) into the integral solution (4.11) and using some simple calculations, one infers

$$I_{eff}^{weak}(x_0 > x_{ps}^{eff}) \approx \pi - \frac{\left(\frac{33}{8} + \frac{471}{128} + \frac{9\pi q^2}{2}\right)}{x_0} + \frac{\left(\frac{741\pi q^2}{32} + \frac{64863\pi}{2048} - \frac{8841q}{1024} - \frac{997q^2}{16}\right)}{x_0^3}.$$
(4.17)

Defining

$$y = \frac{x_0}{x_{ps}^{eff}} > 1 \tag{4.18}$$

and inserting (4.17) the deflection angle (4.1) become

$$\alpha_{eff}^{weak}(y_0 > 1) \approx -\frac{M}{y_0} + \frac{N}{y_0^3}$$
 (4.19)

for weak gravitational lensing where we defined

$$M(x_{ps}^{eff}, q) = \frac{1}{x_{ps}^{eff}} \left(\frac{33}{8} + \frac{471}{128} + \frac{9\pi q^2}{2} \right), \tag{4.20}$$

and

$$N(x_{ps}^{eff}, q) = \frac{1}{(x_{ps}^{eff})^3} \left(\frac{741\pi q^2}{32} + \frac{64863\pi}{2048} - \frac{8841q}{1024} - \frac{997q^2}{16} \right). \tag{4.21}$$

Applying (3.5) and (4.5) we obtain

$$\Omega(x_0) = H, \quad \Omega_1(x_0) = 2H - x_0 H', \quad \Omega_2(x_0) = x_0 H' - H - x_0^2 H''/2$$

$$\Gamma(x) = \Gamma_0(x) = 1, \quad \Gamma_1(x) = 0 = \Gamma_2(x) \tag{4.22}$$

which are applicable for weak deflection angle in absence of NEM field effects. In the latter case asymptotic behavior of the function (4.22) are obtained for $x_0 > x_{ps}$ as follows.

$$\Omega_1(x_0) \approx 2 - \frac{6}{x_0} + \frac{4q^2}{x_0^2} + \frac{15q^2}{x_0^3}$$
(4.23)

and

$$\Omega_2(x_0) \approx -1 + \frac{6}{x_0} - \frac{6q^2}{x_0^2} - \frac{30q^2}{x_0^3}$$
(4.24)

Inserting (4.22), (4.23) and (4.24) one can obtain asymptotic series expansion of the integral solution (4.11) as follows.

$$I^{weak}(x_0) \approx \pi + \frac{3(\pi - 2)}{x_0} + \frac{(8q^2 - 36 - 6\pi q^2 + \frac{27\pi}{2})}{x_0^2} + \frac{(123q^2 - 198 - 42q^2\pi + \frac{135\pi}{2})}{x_0^3}$$

$$(4.25)$$

which by inserting into (4.1) one can obtain weak deflection angle of bending light rays in absence of NEM field such that

$$\alpha^{weak}(y_0 > 1) \approx \frac{S}{y_0} + \frac{R}{y_0^2} + \frac{Q}{y_0^3}$$
 (4.26)

where we defined

$$S(x_{ps}, q) = \frac{3(\pi - 2)}{x_{ps}}, \quad R(x_{ps}, q) = \frac{(8q^2 - 36 - 6\pi q^2 + \frac{27\pi}{2})}{x_{ps}^2}$$
(4.27)

and

$$Q(x_{ps},q) = \frac{(123q^2 - 198 - 42q^2\pi + \frac{135\pi}{2})}{x_{ps}^3}.$$
 (4.28)

Diagrams of the equations (4.19) and (4.26) are plotted in figure 2 for ansatz $y_0 = 10$ by inserting numerical values given in the table 1. It is suitable to obtain the following averaged deflection angles.

$$\sigma_{eff}^{weak} = \bar{\alpha}_{eff}^{weak} \approx -\frac{\bar{M}}{y_0} + \frac{\bar{N}}{y_0^3} \tag{4.29}$$

and

$$\sigma^{weak} = \bar{\alpha}^{weak} \approx \frac{\bar{S}}{y_0} + \frac{\bar{R}}{y_0^2} + \frac{\bar{Q}}{y_0^3}$$

$$\tag{4.30}$$

where we defined all mean coefficients

$$\bar{C} = \frac{1}{N} \sum_{i=1}^{N} C(x_{ps_i}, q_i)$$
 (4.31)

in which $\mathcal{C} = \{M, N, S, R, Q\}$. Inserting numerical values of the table 1 we obtain

$$\bar{M} = 4.79, \quad \bar{N} = 5.41, \quad \bar{S} = 1.32, \quad \bar{R} = 0.64, \quad \bar{Q} = 0.80$$
 (4.32)

for which (4.29) and (4.30) become respectively

$$\sigma_{eff}^{weak}(y_0 > 1) \approx -\frac{4.79}{y_0} + \frac{5.41}{y_0^3}$$
 (4.33)

and

$$\sigma^{weak}(y_0 > 1) \approx \frac{1.32}{y_0} + \frac{0.64}{y_0^2} + \frac{0.80}{y_0^3}.$$
 (4.34)

Diagrams of the above mean weak deflection angles are given in the figure 2. They show that the sign of deflection angle is changed in presence of NEM fields with respect to sign of deflection angle in absence of it.

4.2 Strong lensing deflection angles

In case of strong deflection limits we write Taylor series expansion of the integral solution (4.11) at neighborhood of $x_0 \to x_{ps}^{eff}(y_0 \to 1)$. In the latter case we must be obtain Taylor series expansion of the functions $\Omega_{1,2}(x_0)$ and $\Gamma_{0,1,2}(x_0)$ which up to terms in order of O(3) become respectively

$$\Omega_1(x_0) \approx P_{ps}(y_0 - 1) + Q_{ps}(y_0 - 1)^2,$$
(4.35)

$$\Omega_2(x_0) \approx \Omega_2(x_{ps}) + R_{ps}(y_0 - 1) - Q_{ps}(y_0 - 1)^2$$
(4.36)

$$\Gamma_0(x_0) \approx \Gamma_0(x_{ps}) + U_{ps}(y_0 - 1) + V_{ps}(y_0 - 1)^2,$$
 (4.37)

$$\Gamma_1(x_0) \approx U_{ps} + (U_{ps} + 2V_{ps})(y_0 - 1) + (2V_{ps} + W_{ps})(y_0 - 1)^2,$$
 (4.38)

and

$$\Gamma_2(x_0) \approx U_{ps} + V_{ps} + (U_{ps} + 4V_{ps} + W_{ps})(y_0 - 1) + 3(V_{ps} + W_{ps})(y_0 - 1)^2$$
 (4.39)

where we defined

$$P_{ps} = 2\Omega_2(x_{ps}), \quad \Omega_2(x_{ps}) = \Omega(x_{ps}) - x_{ps}^2 \Omega''(x_{ps})/2$$

$$R_{ps} = -x_{ps}^2 \Omega''(x_{ps}), \quad Q(x_{ps}) = -x_{ps}^3 \Omega'''(x_{ps})/2$$

$$U_{ps} = x_{ps} \Gamma_0'(x_{ps}), \quad V_{ps} = x_{ps}^2 \Gamma_0''(x_{ps})/2, \quad W_{ps} = x_{ps}^3 \Gamma_0'''(x_{ps})/2.$$
 (4.40)

Inserting (4.35), (4.36), (4.37), (4.38) and (4.39) into the integral solution (4.11) one can obtain strong deflection limits of bending light ray angle (4.1) as follows.

$$\alpha_{eff}^{strong}(y_0 \to 1) \approx b + a \ln(y_0 - 1) \tag{4.41}$$

where we defined

$$b = -\pi + \frac{3U_{ps} + 2\ln 2V_{ps}\Gamma_0(x_{ps})}{\sqrt{\Omega_2(x_{ps})}}$$
(4.42)

and

$$a = -\frac{2\Gamma_0(x_{ps})}{\sqrt{\Omega_2(x_{ps})}}. (4.43)$$

Divergency of the above equation in limits $y_0 = 1$ can be described by Bozza formalism as follows.

$$\alpha_{eff}^{strong} = \alpha_n = \Delta \alpha_n + 2n\pi \tag{4.44}$$

where $n=0,\pm 1,\pm 2,\pm 3,\cdots$ means n^{th} circulation of light rays around the lens center to make n^{th} relativistic images by deflecting $0<\Delta\alpha_n<<1$. Non-relativistic images are determined by setting n=0 and relativistic images with positive (negative) parity are determined by setting $n=1,2,\cdots(n=-1,-2,\cdots)$ where one can obtain $\Delta\alpha_{-n}=2\alpha-\Delta\alpha_n$. In case of retro-lensing where observer is located between source and lens, the light rays come back after than that turning around the lens (see figure 1 at ref. [40,41]). In the latter case the parameter 2n given in the formula (4.44) must be replaced with 2n-1. In case of strong deflection limits in absence of NEM fields we should use (4.41) but by inserting

$$P_{ps} = 2H(x_{ps}) - x_{ps}^2 H''(x_{ps}), \quad U_{ps} = -\frac{2x_{ps}H'}{H^3}, \quad V_{ps} = -\frac{x_{ps}^2 H''}{H^3} + \frac{3x_{ps}^2 H'^2}{H^4}$$
(4.45)

and

$$R_{ps} = -x_{ps}^2 H'', \quad Q_{ps} = -x_{ps}^3 H'''/2.$$
 (4.46)

We now study image locations in weak and strong deflection limits.

5 Images locations

In order to calculate the weak deflection images we choose Ohanian lens equation [47] which has high accuracy and so lower errors with respect to other lens equations [55]. It has the advantage of being the closest relative of the exact lens equation, since it only contains the asymptotic approximation without any additional assumptions. It can be rewritten against observational coordinates as image position θ , source position β and deflection angle of bending light rays α^{weak} as follows (see [55] for more discussions).

$$\arcsin(D_L \sin \theta) - \arcsin(D_S \sin \beta) = \alpha - \theta \tag{5.1}$$

in which we defined

$$D_L = \frac{d_{OL}}{d_{LS}}, \quad D_S = \frac{d_{OS}}{d_{LS}}.$$
 (5.2)

In the above equations d_{OS} is distance between observer and source, d_{OL} is distance between the observer and the lens, d_{LS} is distance between the lens and the source. θ is formed when a line passing through the observer and the image is coincide optical axis (line passing through the observer and the lens). β is formed when a line passing through the observer and the source

is coincide the optical axis. One can obtain general solutions of the lens equation (5.1) as follows.

$$\theta_K(\alpha, \beta) = \arctan\left[\frac{D_S \cos \alpha \sin \beta + K \sin \alpha \sqrt{1 - D_S^2 \sin^2 \beta}}{D_L - D_S \sin \alpha \sin \beta + \cos \alpha \sqrt{1 - D_S^2 \sin^2 \beta}}\right]$$
(5.3)

where $K = \pm 1$. It has some real solutions for

$$\sin \beta \le \frac{1}{D_S}.\tag{5.4}$$

In the following we use (5.3) to obtain non-relativistic and relativistic image locations.

5.1 Weak lensing images

In weak deflection limits with large distances between lens, source and observer located in a straight line approximately, one can infer [55]

$$D_S \approx D_L + 1. \tag{5.5}$$

where $D_L >> 1$ must be inserted via experimental date. As a realistic example of gravitational lens we consider a big black hole located in the center of Galaxy and study image locations of a star located far from it. This black hole is called as Sgr A* [48-51]. Its mass is estimated as $3.6 \times 10^6 M_{\odot}$ and its distance from the earth is $d_{OL} = 8kpc = 2.47 \times 10^{17} m$ with corresponding Schwarzschild radius $R_{SCH} = 10^{10} m$. We consider a source to be a star located at distance $d_{LS} = 1.7 \times 10^{13} m$ from the black hole which is far from the margin of the accretion disk of the black hole, so it may not be fall toward the black hole center. For the latter black hole we will have

$$D_L \approx 1.45 \times 10^4 \approx D_S. \tag{5.6}$$

The relations (5.4) and (5.6) leads us to choose

$$\sin \beta \approx \beta \le \beta_M,\tag{5.7}$$

in weak deflection limits of gravitational lensing where we defined

$$\beta_M = \frac{1}{D_S} \approx \frac{1}{D_L} \approx 7 \times 10^{-5} Rad \equiv 40107 \mu \ arc \ sec \tag{5.8}$$

in which the subscript M denotes to the word 'Maximum'. For critical source $\beta = \beta_M$ the lens equation (5.3) reads

$$\theta_M(\alpha) = \arctan\left[\frac{\cos\alpha}{D_L - \sin\alpha}\right]$$
 (5.9)

which for weak deflection limits $\alpha \to 0$ leads to the following approximation.

$$\theta_M \approx \frac{1}{D_L} \approx 40107 \mu \ arc \ sec.$$
 (5.10)

Defining

$$\theta^* = \frac{\theta}{\theta_M}, \quad \beta^* = \frac{\beta}{\beta_M} \tag{5.11}$$

we can obtain Taylor series expansion of the lens equation (5.3) at neighborhood of $(|\alpha|, |\beta^*|) \ll (1, 1)$ as follows.

$$\theta_K^* \approx \frac{KD_L}{1+D_L}\alpha + \frac{D_L}{1+D_L}\beta^* - \frac{K}{6}\frac{D_L^2(D_L-1)}{(1+D_L)^3}\alpha^3$$

$$-\frac{D_L}{2}\frac{D_L^2 - 2KD_L + 2 + D_L - 2K}{(1+D_L)^3}\beta^*\alpha^2$$

$$-\frac{D_L}{2}\frac{(D_L^2K + D_LK - 2D_L + 2K - 2)}{(1+D_L)^3}\alpha\beta^{*2} + \frac{D_L}{6}\frac{1+3D_L}{(1+D_L)^3}\beta^{*3}$$

$$+\frac{KD_L}{120}\frac{(D_L^4 + 11D_L^2 - 11D_L^3 - D_L)}{(1+D_L)^5}\alpha^5 + \cdots$$
 (5.12)

which in limits $D_L \to \infty$ become

$$\theta_K^* \approx K\alpha + \beta^* - \frac{\alpha^2 \beta^*}{2} - \frac{K\alpha \beta^{*2}}{2} - \frac{K}{6}\alpha^3 + \frac{K}{120}\alpha^5 + \cdots$$
 (5.13)

This is primary image location and by transforming $\beta^* \to -\beta^*$ as $\theta_K^*(-\beta^*)$ one can obtain secondary image location. The parameter $K=\pm 1$ describes right-handed (+1)and/or left-handed (-1) bending angles. Setting $K=+1,\beta^*=1,y_0=10$ and inserting numerical values of the deflection angles (4.19) and (4.26) via numerical values of the table 1 (see diagrams of the figure 2) we plot numerical values of θ_i^{eff} and θ_i against different values of $|q_i|$ in figure 3. Also we insert (4.33) and (4.34) into the weak lens equation (5.13) by setting K=+1 and plot mean weak image locations in figure 3 against |q| in figure 3. We now obtain relativistic image locations.

5.2 Strong lensing images

The Virbhadra-Ellis lens equation given by [56]

$$\tan \beta = \tan \theta - D[\tan(\alpha - \theta) + \tan \theta] \tag{5.14}$$

is useful to study gravitational lensing in strong field limits. In the above lens equation we have $D=\frac{d_{ls}}{d_{os}}$ for standard lensing in which lens is located between observer and source, $D=\frac{d_{os}}{d_{ol}}$ for situations where the source is located between observer and lens, and with $D=\frac{d_{os}}{d_{ls}}$ for situations where the observer is located between the source and the lens (the retro-lensing). The lensing effects are more important when the objects are highly aligned, in which β , θ are small and α is close to $2n\pi + \Delta \alpha_n$ (standard lensing) and/or $(2n+1)\pi + \Delta \alpha_n$ (retro-lensing) with $0 < \Delta \alpha_n << 1$, $n=1,2,\cdots$. In the latter case we can use the approximations $\tan \theta \approx \theta$ and $\tan \beta \approx \beta$ for the lens equation (5.14) and insert $\alpha = 2n\pi + \Delta \alpha_n$ such that (see Eq. 32 in ref. [52])

$$\beta = \theta - D\Delta \alpha_n. \tag{5.15}$$

Defining coordinate independent impact parameter

$$u = \frac{r}{\sqrt{\Omega(r)}},\tag{5.16}$$

one can obtain its Taylor series expansion as (see Eq.28 in Ref. [52])

$$y_0 - 1 \approx \sqrt{2} \left(\frac{\Omega_2(x_{ps})}{\Omega(x_{ps})} \right)^{-\frac{1}{2}} \left(\frac{u_0}{u_{ps}} - 1 \right)^{\frac{1}{2}}$$
 (5.17)

in which $u_0 = d_{LO} \sin \theta$ reading to $u_0 \approx d_{LO} \theta$ for small θ . Inserting the latter relation and (5.17), the strong deflection angle (4.41) become

$$\alpha(\theta) = c_2 - c_1 \ln \left(\frac{d_{OL}}{u_{ps}} \theta - 1 \right)$$
 (5.18)

where we defined

$$c_1 = -\frac{a}{2}, \quad c_2 = b + \frac{a}{2} \ln \left(\frac{2\Omega(x_{ps})}{\Omega_2(x_{ps})} \right).$$
 (5.19)

One can obtain $\theta(\alpha)$ by inverting (5.18) as

$$\theta(\alpha) = \frac{u_{ps}}{d_{OL}} (1 + e^{(c_2 - \alpha)/c_1})$$
 (5.20)

and inserting (4.44) can be rewritten as

$$\theta_n = \frac{u_{ps}}{d_{OL}} (1 + e^{(c_2 - 2n\pi - \Delta\alpha_n)/c_1}). \tag{5.21}$$

Making first order Taylor series expansion of the above equation around $\alpha = 2n\pi$ the angular position of n^{th} relativistic image is obtained as

$$\theta_n \approx \theta_n^{(0)} - \zeta_n \Delta \alpha_n \tag{5.22}$$

where we defined

$$\theta_n^{(0)} = \frac{u_{ps}}{d_{OL}} [1 + e^{(c_2 - 2n\pi)/c_1}]$$
(5.23)

and

$$\zeta_n = \frac{u_{ps}}{c_1 d_{OL}} e^{(c_2 - 2n\pi)/c_1}.$$
 (5.24)

Eliminating $\Delta \alpha_n$ between (5.15) and (5.22) we obtain

$$\theta_n = \left(1 + \frac{\zeta_n}{D}\right)^{-1} \left(\theta_n^{(0)} + \frac{\zeta_n}{D}\beta\right) \tag{5.25}$$

in which $0 < \zeta_n/D << 1$ and so we can use approximation $(1 + \frac{\zeta_n}{D})^{-1} \approx 1 - \frac{\zeta_n}{D}$. In the latter case the equation (5.25) reads

$$\theta_n \approx \theta_n^{(0)} + \frac{\zeta_n}{D} (\beta - \theta_n^{(0)}). \tag{5.26}$$

The second term in the above lens equation is more smaller than the first term which means all relativistic image locations lie very close to $\theta_n^{(0)}$. There are other set of relativistic images by changing $\theta_n^{(0)} \to -\theta_n^{(0)}$ into the above lens equation. In case of perfect aligned $\beta=0$ the above lens equation reaches to

$$\theta_n^E = \left(1 - \frac{\zeta_n}{D}\right) \theta_n^{(0)} \tag{5.27}$$

describing n^{th} relativistic Einstein ring.

5.2.1 Magnifications

The magnification μ of an image is defined as the ratio of flux of the image to flux of un-lensed source. It has two components called as tangential $\mu_t = \frac{\sin \theta}{\sin \beta}$ and radial $\mu_r = \frac{d\theta}{d\beta}$ which their multiplication makes the magnification as

$$\mu = \left| \frac{\sin \beta}{\sin \theta} \frac{d\beta}{d\theta} \right|^{-1}.$$
 (5.28)

The above equation denotes to primary image $\theta^p(\beta)$ magnifications with positive parity. Inserting the secondary image location $\theta^s(\beta) = \theta^p(-\beta)$ into the magnification equation (5.28) one can obtain secondary image magnification $\mu^s_{weak}(\beta) = \mu^p_{weak}(-\beta)$ with negative parity. In the micro-lensing state two weak field images are not resolved and so the main observables should be considered become the total magnification μ_{tot} and magnification-weighted-centroid μ_{cent} defined by respectively [57]

$$\mu_{tot} = |\mu_s| + |\mu_p| \tag{5.29}$$

and

$$\mu_{cent} = \frac{\theta_p |\mu_p| + \theta_s |\mu_s|}{|\mu_p| + |\mu_s|}.$$
 (5.30)

We now calculate the above magnifications for weak and strong lensing.

5.3 Weak lensing magnifications

In case of weak deflection limits we can use $\sin \theta \approx \theta$ and $\sin \beta \approx \beta$ to evaluate (5.28) as follows.

$$\mu^{weak} \approx \left| \frac{\beta}{\theta} \frac{d\beta}{d\theta} \right|^{-1} \tag{5.31}$$

which by inserting (5.13) reads

$$\mu_K^{weak} \approx \left| K\alpha + \beta^* - \frac{\alpha^2 \beta^*}{2} - \frac{K\alpha \beta^{*2}}{2} - \frac{K\alpha^3}{6} + \frac{K\alpha^5}{120} \right| \times \left| \frac{1}{\beta^*} - \frac{\alpha^2}{2\beta^*} - K\alpha \right|. \tag{5.32}$$

Inserting numerical values given in the table 2 we calculate numerical values of μ , μ_{tot} , μ_{cent} to plot their diagrams against β^* in figure 4. Diagrams show that μ decreases by increasing |q| in presence and absence of NEM fields. μ_{tot} has minimum value for $\beta > 0 (\beta < 0)$ in presence (absence) of NEM fields. While corresponding μ_{cent} take maximum value. Furthermore we see from the figure 4 that magnification of the Einstein rings is major in presence of NEM fields with respect to situations where there is not. We now study strong lensing magnifications.

5.3.1 Strong lensing magnifications

We now are in position to calculate n^{th} relativistic images magnification which is determined by

$$\mu_n \approx \left| \frac{\beta}{\theta_n} \frac{d\beta}{d\theta_n} \right|^{-1} \tag{5.33}$$

and by inserting (5.26) reads

$$\mu_n \approx \frac{\zeta_n}{D} \frac{\theta_n^{(0)}}{\beta}.\tag{5.34}$$

The above magnification is valid for a point source and for extended source there is obtained a different form of the magnification (see for instance Eq. (46) in Ref. [52]). The equation (5.34) shows that the first relativistic image is brightest one, and the magnifications decreases exponentially with 'n'. Magnifications in case of retro-lensing is obtained by (5.34) but by changing $2n \to 2n - 1$. The total magnification, taking into account both sets of relativistic images, is defined by $\mu_{tot}^{strong} = 2\sum_{n=1}^{\infty} \mu_n$. Using the formula $\frac{t}{1-t} = \sum_{n=1}^{\infty} t^n$ and inserting (5.23), (5.24) and (5.34) we obtain

$$\mu_{tot}^{strong} = \frac{1}{\beta} \left(\frac{2u_{ps}^2 e^{\frac{c_2}{c_1}}}{Dc_1 d_{OL}^2} \right) \left[\frac{1 + e^{\frac{c_2}{c_1}} + e^{\frac{2\pi}{c_1}}}{e^{\frac{4\pi}{c_1}} - 1} \right]$$
(5.35)

for a point source where

$$u_{ps}(x_{ps}) = \frac{x_{ps}}{\sqrt{\Omega(x_{ps})}},\tag{5.36}$$

$$c_1(x_{ps}) = \frac{\Gamma_0(x_{ps})}{\sqrt{\Omega_2(x_{ps})}},$$
 (5.37)

and

$$c_2(x_{ps}) = -\pi + \frac{3U_{ps} + V_{ps} + 2\ln 2\Gamma_0(x_{ps})}{\sqrt{\Omega_2(x_{ps})}} - \frac{\Gamma_0(x_{ps})}{\sqrt{\Omega_2(x_{ps})}} \ln \left[\frac{2\Omega(x_{ps})}{\Omega_2(x_{ps})}\right]. (5.38)$$

The equations (5.37) and (5.38) are obtained by inserting (4.42) and (4.43) into the relations (5.19).

As an example we obtain the lensing observable defined by Bozza [37] as

$$s = \theta_1 - \theta_\infty \tag{5.39}$$

and

$$r = \frac{\mu_1}{\sum_{n=2}^{\infty} \mu_n} \tag{5.40}$$

which are useful when the outermost relativistic image can be resolved from the rest. 's' represents the angular separation between the first image and the limiting value of the succession of images. 'r' is the ratio between the flux of the first image and sum of the fluxes of the other images. Applying (5.24) and (5.26) one can obtain exact form of the equation (5.39) which up to term of $0 < \frac{\zeta_1}{D} << 1$ become

$$s \approx \theta_{\infty} e^{(c_2 - 2\pi)/c_1} \tag{5.41}$$

in which

$$\theta_{\infty} = \frac{u_{ps}}{\tilde{d}_{OL}} \tag{5.42}$$

and numerical value of \tilde{d}_{LO} is used here for Sgr A^* observed galactic black hole as

$$\tilde{d}_{OL} = \frac{d_{OL}}{R_{SCH}} = \frac{2.47 \times 10^{17} m}{10^{10} m} = 2.47 \times 10^7$$
 (5.43)

One infers that the equation (5.40) can be rewritten as

$$r = \frac{2\mu_1}{\mu_{tot}^{strong} - 2\mu_1} \tag{5.44}$$

which by inserting (5.34) and (5.35) reads

$$r = \frac{e^{\frac{2\pi}{c_1}} + e^{\frac{c_2}{c_1}} - e^{-\frac{2\pi}{c_1}} + e^{\frac{c_2}{c_2}} e^{-\frac{4\pi}{c_1}}}{1 + e^{-\frac{2\pi}{c_1}} - e^{\frac{c_2}{c_1}} e^{-\frac{4\pi}{c_1}}}$$
(5.45)

and its Taylor series expansion about $e^{-\frac{2\pi}{c_1}} \to 0$ become

$$r \approx e^{\frac{2\pi}{c_1}} + e^{\frac{c_2}{c_1}} - 1.$$
 (5.46)

We plot diagrams of $c_{1,2}$ against |q| in figure 5 for |q| < 1 and figure 7 for |q| > 1. They show raise of $c_{1,2}$ to large negative values in absence of NEM fields. While in presence of NEM fields c_1 takes some positive values for |q| < 0.6 and reaches to negative values for 0.6 < |q| < 1. c_2 decreases by increasing |q| < 1 in presence of NEM fields. For |q| > 1 the diagrams of the figure 7 shows increase of $c_1(c_2)$ to some positive (negative) values by

decreasing |q| > 1 in absence (presence) of NEM fields. r(s) behaves as increasing (decreasing) function by raising |q| > 1. In figure 6 we see increase (decrease) of s by raising |q| < 1 in absence (presence) of NEM fields. r decreases (increase) by raising |q| < 1 in absence (presence) of the NEM fields.

6 Concluding remark

As a black hole solution of Born Infeld Einstein-non linear Maxwell gravity we use ABG nonsingular charged black hole to study its gravitational lensing in weak and strong deflection limits. We set our calculations to Sgr A* observed black hole date and study non linear counterpart of EM field on the gravitational lensing. In short we obtained negligibility of NEM effects for large values of the black hole charge but not for its small values. Nonlinearity causes to be larger the photon sphere radius. Sign of deflection angle of bending light rays is changed. Einstein rings become larger and their magnifications become greater. Angular separation of innermost and outermost relativistic images decreases by increasing the charge parameter but their magnifications increase. As a future work one can use strategy and results of this work to compare with results obtained by studying gravitational lensing of other nonsingular galactic black holes described in the introduction section and setting other observed black holes data.

References

- 1. S. W. Hawking and G. F. R. Ellis, *The large scale structure of space-time*, (Cambridge University Press, England, 1973).
- 2. R. M. Wald, *General relativity*, (The University of Chicago, Chicago Press, 1984).
- **3.** R. M. Wald, *Gravitational collapse and cosmic censorship*, In black holes, gravitational radiation and the Universe, (Springer, Netherlands, 1999).
- 4. I. Dymnikova, "Spherically symmetric space-time with the regular de Sitter center," Int. J. Mod. Phys. D12, 1015 (2003).
- **5.** A. A. Tseytlin, "On singularities of spherically symmetric backgrounds in string theory," Phys. Lett. B**363**, 223 (1995).

- **6.** M. Cvetic, "Flat world of dilatonic domain walls," Phys. Rev. Lett. **71**, 815 (1993).
- 7. J. H. Horne and G. T. Horowitz, "Exact black string solutions in three-dimensions," Nucl. Phys. B368, 444 (1992).
- 8. K. A. Bronnikov, V. N. Melnikov and H. Dehnen, "Regular black holes and black universes," Gen. Rel. Grav. 39, 973 (2007).
- **9.** S. Ansoldi, "Spherical black holes with regular center", gr-qc/0802.0330 (2008).
- 10. J. Bardeen, Proceedings of GR5, Tiflis, USSR, (1968).
- 11. E. Ayon-Beato and A. Garcia, "The Bardeen model as a nonlinear magnetic monopole," Phys. Lett. B493, 149 (2000); gr-qc/0009077.
- 12. E. Ayon-Beato and A. Garcia, "Regular black hole in general relativity coupled to nonlinear electrodynamics," Phys. Rev. Lett. 80, 5056 (1998), gr-qc/9911046v1.
- **13.** E. Ayon-Beato and A. Garcia, "New regular black hole solution from nonlinear electrodynamics," Phys. Lett. B**464**, 25 (1999).
- **14.** E. Ayon-Beato and A. Garcia, "Nonsingular charged black hole solution for nonlinear source," Gen. Rel. Grav. **31**, 629 (1999).
- **15.** S. A. Hayward, "Formation and evaporation of regular black holes," Phys. Rev. Lett. **96**, 031103 (2006).
- **16.** J. C. S. Neves and A. Saa, "Regular rotating black holes and the weak energy condition," Phys. Lett. B**734**, 44 (2014); gr-qc/1402.2694.
- **17.** J. C. S. Neves, "Note on regular black holes in a brane world," Phys. Rev. D**92**, 084015 (2015); gr-qc/1508.0361.
- 18. M. Azreg-Ainou, "Generating rotating regular black hole solutions without complexification," Phys. Rev. D90, 064041 (2014).
- **19.** C. Bambi and L. Modesto, "Rotating regular black holes," Phys. Lett. B**721**, 329 (2013); gr-qc/1302.6075.

- 20. B. Toshmatov, B. Ahmedov, A. Abdujabbarov and Z. Stuchlik, "Rotating regular black hole solution," Phys. Rev. D89, 104017 (2014); gr-qc/1404.6443.
- **21.** Sushant G. Ghosh "A nonsingular rotating black hole," EPJ. C**75**, 532, (2015).
- 22. E. F. Eiroa and C. M. Sendra, "Regular phantom black hole gravitational lensing," Phys. Rev. D88, 103007 (2013).
- 23. L. Modesto and P. Nicolini, "Charged rotating noncommutative black holes," Phys. Rev. D82, 104035 (2010); gr-qc/1005.5605.
- **24.** Sushant G. Ghosh, P. Sheoran and M. Amir "Rotating Ayon-Beato-Garcia black hole as a particle accelerator," Phys. Rev. D**90**,103006 (2014); gr-qc/1410.5588.
- 25. G. V. Kraniotis, "Gravitational lensing and frame dragging of light in the Kerr-Newman and the Kerr-Newman-(anti) de Sitter black hole space time", Gen. Rel. Grav. 46 11, 1818 (2014).
- 26. M. Patil and P. S. Joshi, "Ultra-high energy particle collisions in a regular space time without black holes or naked singularities," Phys. Rev. D86, 044040 (2012).
- 27. Z. Stuchlik, J. Schee and A. Abdujabbarov, "Ultra-high-energy collisions of particles in the field of near-extreme Kehagias-Sfetsos naked singularities and their appearance to distant observers," Phys. Rev. D89, 104048 (2014).
- 28. A. Garca, E. Hackmann, J. Kunz, C. Lmmerzahl and A. Macas, "Motion of test particles in a regular black hole spacetime," J. Math. Phys. 56, 032501 (2015).
- **29.** Z. Stuchlik and J. Schee, "Circular geodesic of Bardeen and Ayon-Beato-Garcia regular black-hole and no-horizon spacetimes," Int. J. Mod. Phys. D**24**, 1550020 (2015).
- **30.** Z. Stuchlik and J. Schee, "Optical effects related to Keplerian discs orbiting Kehagias-Sfetsos naked singularities," Class. Quant. Grav. **31**, 195013 (2014).

- **31.** J. Schee and Z. Stuchlik, "Profiled spectral lines generated by Keplerian discs orbiting in the Bardeen and Ayon -Beato-Garcia space times", Class. Quantum Grav., **33**, 085004, (2016).
- **32.** A. Kehagias and K. Sfetsos, "The Black hole and FRW geometries of non-relativistic gravity," Phys. Lett. B**678**, 123 (2009).
- **33.** E. F. Eiroa, G. E. Romero and D. F. Torres, "Reissner-Nordstrom black hole lensing," Phys. Rev. D**66**, 024010 (2002).
- **34.** E. F. Eiroa and C. M. Sendra, "Gravitational lensing by a regular black hole," Class. Quant. Grav. **28**, 085008 (2011).
- **35.** S. W. Wei, Y. X. Liu and C. E. Fu, "Null geodesics and gravitational lensing in a nonsingular spacetime," Adv. High Energy Phys. **2015**, 454217 (2015).
- **36.** H. Ghaffarnejad and H. Niad, "Weak gravitational lensing from regular Bardeen black holes," Int. J. Theor. Phys. **54**, 9, 1 (2015); gr-qc/1411.7247.
- **37.** V. Bozza, "Gravitational lensing in the strong field limit," Phys. Rev. D**66**, 103001 (2002); gr-qc/0208075.
- **38** V. Bozza, "Gravitational lensing by black holes," Gen. Rel. Grav. **42**, 2269 (2010).
- **39.** S. Sahu, K. Lochan and D. Narasimha, 'Gravitational lensing by self-dual black hole in loop quantum gravity' Phys. Rev. **D91**, 063001 (2015).
- **40.** E. F. Eiroa and D. F. Torres, "Strong field limit analysis of gravitational retro lensing," Phys. Rev. D**69**, 063004 (2004); gr-qc/0311013.
- **41.** E. F. Eiroa, 'Braneworld black hole gravitational lensing: Strong field limits analysis', Phys. Rev D**71**, 083010 (2005).
- **42.** S. Sahu, M. Patil, D. Narasimha and P. S. Joshi, "Can strong gravitational lensing distinguish naked singularities from black holes?," Phys. Rev. D**86**, 063010 (2012).

- **43.** R.R.Cuzinato, C.A.M.de Melo, K.C. de Vasconcelos, L. G. Medeiros and P. J. Pompeia, "Nonlinear effects on radiation propagation around a charged compact object", Astrophys. Space Sci 359, 59 (2015).
- **44.** M. Novello, V. A. de Lorenci, J. M. Salim and R. Klippert, "Geometrical aspects of light propagation in nonlinear electrodynamics", Phys. Rev. D61, 045001 (2000).
- **45.** N. Breton, "Geodesic structure of the Born-Infeld black hole" Class. Quantum Grav. 19, 601, (2002).
- **46.** H. Ghaffarnejad "Classical and quantum Reissner Nordström black hole thermodynamics and first order phase transition," Astrophys. Space Sci. **361**, 7, 1 (2016); physics.gen-ph/1308.1323.
- **47.** H. C. Ohanian, "The black holes as a gravitational lens", Am. J. Physics **55** (5), 428 (1987).
- **48.** R. Genzel et al, "The Galactic Center massive black hole and nuclear star cluster", Rev.Mod. Phys. **82** 3121-95 (2010).
- **49.** A. M. Ghez et al, "Measuring distance and properties of the Milky Ways central supermassive black hole with stellar orbits", Astrophys. J. **689**, 1044 (2008).
- **50.** F. Melia *The black hole at the center of our Galaxy*, (Princeton University Press, Princeton 2003).
- 51. F. Eisenhauer et al., "SINFONI in the Galactic Center: Young Stars and Infrared Flares in the Central Light-Month", Astrophys. J. 628, 246 (2005).
- **52.** E. F. Eiroa, "Gravitational lensing by Einstein-Born-Infeld black holes" Phys. Rev. D73, 043002 (2006); gr-qc/0511065v2.
- **53.** C. M. Claudel, K. S. Virbhadra and G. F. R. Ellis, "The geometry of photon surfaces," J. Math. Phys. **42**, 818 (2001).
- **54.** S. Weinberg, Gravitation and Cosmology: Principle and Applications of the General Theory of Relativity (Wiley New York 1972).

- **55.** V. Bozza, "Comparison of approximate gravitational lens equations and a proposal for an improved new one" Phys. Rev. D78, 103005 (2008).
- **56.** K. S. Virbhadra and G. F. R. Ellis, "Schwarzschild black hole lensing", Phys. Rev. D62, 0840 03 (2000).
- 57 B. S. Gaudi and A. O. Petters, "Gravitational Microlensing Near Caustics II: Cusps", Astrophys. J. 580, 468-489 (2002), astro-ph/0206162.

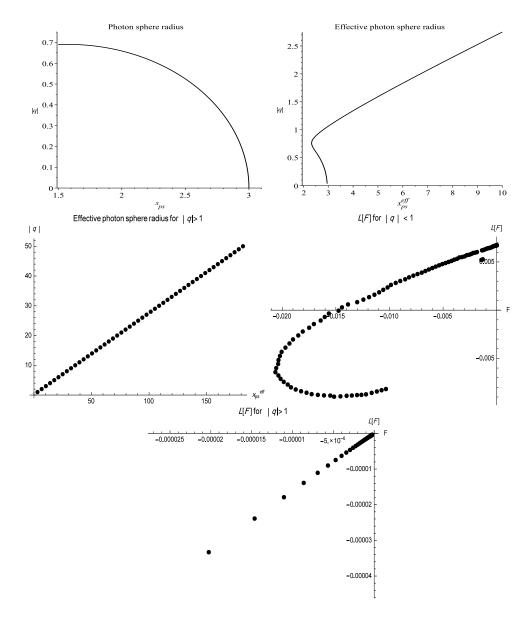


Figure 1: Diagrams of photon sphere locations x_{ps} and NEM field lagrangian density L[F]

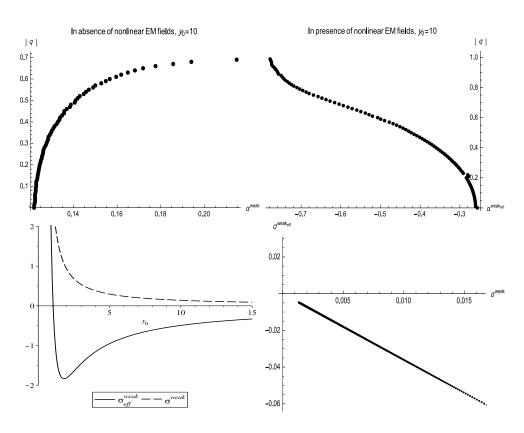


Figure 2: Diagrams of weak lensing deflection angles for $|\boldsymbol{q}|<1$

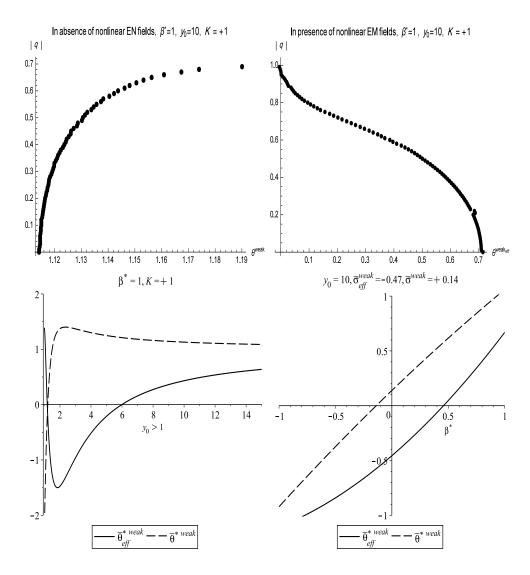


Figure 3: Diagrams of weak lensing primary image locations for $\vert q \vert < 1$

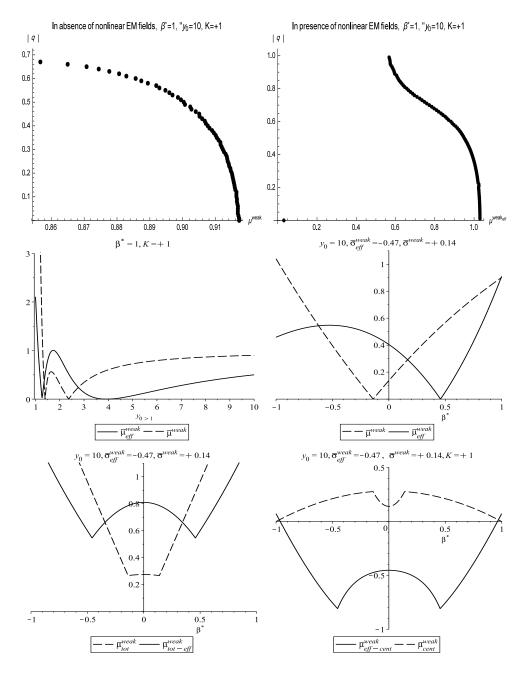


Figure 4: Diagrams of weak lensing image magnifications for |q| < 1

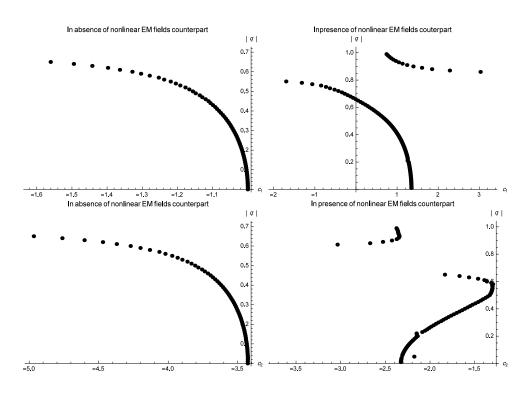


Figure 5: Diagrams of c_1, c_2 are plotted against |q| < 1.

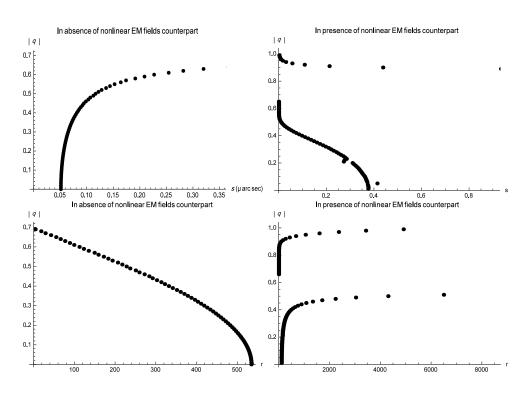


Figure 6: Diagrams of s, r are plotted against |q| < 1.

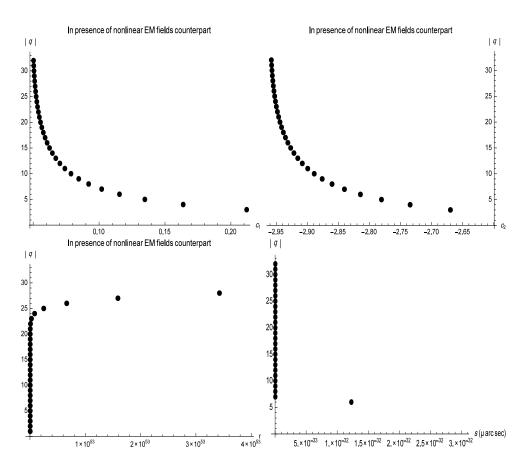


Figure 7: Diagrams of c_1, c_2, s, r are plotted against |q| > 1.

Table 1. Numerical major real roots of the photon sphere equations (3.17) and (3.19) for 0 < |q| < 1.

$ q , x_{ps}, x_{ps}^{eff}$	$ q $, x_{ps} , x_{ps}^{eff}	$ q $, x_{ps} , x_{ps}^{eff}	$ q $, x_{ps} , x_{ps}^{eff}
0.00, 3.000, 3.000	0.25, 2.892,2.874	0.50, 2.547, 2.645	0.75,-,2.326
0.01, 2.999, 2.950	0.26, 2.887, 2.871	0.51, 2.528,2.640	0.76, -,2.320
0.02, 2.994, 2.947	0.27, 2.882, 2.865	0.52, 2.508, 2.630	0.77, -,2.326
0.03, 2.989, 2.947	0.28, 2.872, 2.855	0.53, 2.475, 2.621	0.78, -,2.329
0.04, 2.989, 2.947	0.29, 2.858, 2.852	0.54, 2.455, 2.609	0.79, -, 2.335
0.05, 2.989, 2.944	0.30, 2.848, 2.843	0.55, 2.431, 2.594	0.80, -,2.344
0.06, 2.989, 2.943	0.31, 2.838, 2.831	0.56, 2.397, 2.578	0.81, -,2.350
0.07, 2.984, 2.942	0.32, 2.828, 2.828	0.57, 2.378, 2.560	0.82, -, 2.362
0.08,2.980, 2.941	0.33, 2.824, 2.819	0.58, 2.334, 2.530	0.83, -, 2.377
0.09, 2.980, 2.938	0.34, 2.809, 2.813	0.59, 2.300, 2.514	0.84, -, 2.393
0.10, 2.975, 2.935	0.35, 2.795,2.804	0.60, 2.271,2.508	0.85, -,2.408
0.11, 2.974, 2.935	0.36, 2.785, 2.795	0.61, 2.227,2.478	0.86, -,2.429
0.12, 2.974, 2.935	0.37, 2.770,2.785	0.62, 2.193, 2.469	0.87, -, 2.451
0.13, 2.964, 2.932	0.38, 2.756, 2.776	0.63, 2.150,2.460	0.88, -, 2.475
0.14, 2.959, 2.928	0.39, 2.736, 2.767	0.64, 2.106, 2.441	0.89, -, 2.487
0.15, 2.955, 2.925	0.40, 2.722, 2.758	0.65, 2.058,2.429	0.90, -,2.514
0.16, 2.950, 2.919	0.41, 2.707, 2.749	0.66, 1.990, 2.411	0.91, -, 2.542
0.17, 2.945, 2.916	0.42, 2.698, 2.740	0.67, 1.902,2.399	0.92, -, 2.566
0.18, 2.940, 2.913	0.43, 2.678, 2.731	0.68, 1.819,2.384	0.93, -, 2.591
0.19, 2.935, 2.910	0.44, 2.659,2.718	0.69, 1.645, 2.374	0.94, -, 2.612
0.20, 2.930, 2.904	0.45, 2.654, 2.706	0.70, -, 2.362	0.95, -, 2.636
0.21, 2.921, 2.989	0.46, 2.630, 2.694	0.71, -, 2.350	0.96, -,2.670
0.22, 2.916,2.895	0.47, 2.601, 2.685	0.72, -, 2.344	0.97, -,2.703
0.23, 2.906, 2.889	0.48, 2.591,2.670	0.73, -, 2.338	0.98, -, 2.734
0.24, 2.901, 2.883	0.49, 2.557, 2.658	0.74, -,2.335	0.99, -, 2.764

Table 2. Solutions of the effective photon sphere equation (3.20) for |q| > 1.

| $ q , x_{ps}^{eff}$ |
|---------------------|---------------------|---------------------|---------------------|---------------------|---------------------|
| 1, 2.847 | 7, 24.705 | 13,46.563 | 19, 68.421 | 25, 90.279 | 31, 112.137 |
| 2, 6.490 | 8, 28.348 | 14,50.206 | 20, 72.064 | 26, 93.922 | 32, 115.780 |
| 3, 10.133 | 9, 31.991 | 15,53.849 | 21, 75.707 | 27, 97.565 | 33, 119.423 |
| 4, 13.776 | 10, 35.634 | 16,57.492 | 22, 79.350 | 28, 101.208 | 34, 123.066 |
| 5, 17.419 | 11, 39.277 | 17, 61.135 | 23,82.993 | 29, 104.851 | 35, 126.709 |
| 6, 21.062 | 12, 42.920 | 18,64.778 | 24,86.636 | 30, 108.494 | 36, 130.352 |